

Picosecond pulse-shaping for strong three-dimensional field-free alignment of generic asymmetric-top molecules

Terry Mullins,¹ Evangelos T. Karamatskos,^{1,2} Joss Wiese,^{1,3,4} Jolijn Onvlee,^{1,4}
Arnaud Rouzée,⁵ Andrey Yachmenev,^{1,4} Sebastian Trippel,^{1,4} and Jochen Küpper^{1,2,3,4,*}

¹Center for Free-Electron Laser Science, Deutsches Elektronen-Synchrotron DESY, Notkestraße 85, 22607 Hamburg, Germany

²Department of Physics, Universität Hamburg, Luruper Chaussee 149, 22761 Hamburg, Germany

³Department of Chemistry, Universität Hamburg, Martin-Luther-King-Platz 6, 20146 Hamburg, Germany

⁴Center for Ultrafast Imaging, Universität of Hamburg, Luruper Chaussee 149, 22761 Hamburg, Germany

⁵Max Born Institute, Max-Born-Straße 2a, 12489 Berlin, Germany

(Dated: 2024-04-03)

We demonstrate three-dimensional (3D) field-free alignment of the prototypical non-rotation-symmetric molecule indole using elliptically polarized, shaped, off-resonant laser pulses. A truncated laser pulse is produced using a combination of extreme linear chirping and controlled phase and amplitude shaping using a spatial-light-modulator (SLM) based pulse shaper of a broadband laser pulse. The angular confinement is detected through velocity-map imaging of H^+ and C^{2+} fragments resulting from strong-field ionization and Coulomb explosion of the aligned molecules by intense femtosecond laser pulses. The achieved three-dimensional alignment is characterized by comparing the result of ion-velocity-map measurements for different alignment directions and for different times during and after the alignment laser pulse to accurate computational results. The achieved strong three-dimensional field-free alignment of $\langle \cos^2 \delta \rangle = 0.89$ demonstrates the feasibility of both, strong three-dimensional alignment of generic complex molecules and its quantitative characterization.

Laser-induced alignment of gas-phase molecules has proven to be an efficient way to access the molecular frame [1, 2]. It was extensively used in high-harmonic-generation-spectroscopy [3, 4], strong-field-ionization [5–7], x-ray-diffraction [8, 9] and electron-diffraction [10–14] experiments, enabling the imaging of molecular structure and dynamics directly in the molecular frame. Furthermore, it was crucial for retrieving the shapes of molecular orbitals [15–17].

Such advanced imaging technologies are especially important for complex molecules, i.e., asymmetric tops without any rotational symmetry, which is the case for almost all molecules on earth. Thus it is of utmost importance to develop laser alignment into a practical tool for such molecules. This would, for instance, maximize the information content of atomic-resolution imaging experiments [18, 19], as already suggested for the coherent diffractive x-ray imaging of biological macromolecules more than fifteen years ago [20]. In order to minimize perturbations by external fields this should be achieved in a laser-field-free environment. The associated problems are twofold: The rotational dynamics of these non-rotation-symmetric molecules are very complicated and incommensurate [21, 22]. Moreover, the standard approaches to characterize the 3D degree of alignment, using ion imaging of atomic fragments, mostly halogen atoms, recoiling along a well-defined molecular axis, do not work.

One-dimensional alignment of linear and (near) symmetric top molecules has been demonstrated extensively and really pushed to the limits [1, 2, 16, 23–26]. Furthermore, also the three-dimensional (3D) control of rotation-symmetric molecules, typically during long laser pulses, was demonstrated by multiple groups, making use of

highly polarizable halogen atoms for large polarizability effects as well as their symmetric fragmentation dynamics for characterization [16, 27–32]. This was extended to the field-free 3D alignment of molecules in helium nanodroplets [33] and to the alignment of one slightly non-rotation-symmetric molecule 6-chloropyridazine-3-carbonitrile using long laser pulses [21, 34].

Here, we demonstrate and characterize the strong laser-field-free three-dimensional alignment of the prototypical (bio)molecule indole (C_8H_7N , Figure 1 a), a good representative of the general class of molecules without any rotational symmetry and without any good leaving-group fragments for standard characterization. We use a combination of a shaped, truncated, elliptically-polarized laser pulse with a short kick pulse before truncation to induce strong three-dimensional alignment. The degree of alignment is characterized through strong-field multiple ionization and subsequent velocity-map imaging (VMI) of H^+ , C^+ , C^{2+} , and CH_xN^+ ($x=0,1,2$) fragments, combined with computational results to disentangle the temporal and angular dependence of the alignment. Our approach shows that the molecular frame even of molecules without rotational symmetry can be accessed.

The experimental setup was described elsewhere [35]. Briefly, molecules were cooled in a supersonic expansion from a pulsed Even-Lavie valve [36], operated at a temperature of 80 °C and at a repetition rate of 100 Hz. Around 1.4 mbar of indole was seeded in 95 bar of He, which was expanded into vacuum. The lowest-energy rotational states were selected using an electrostatic deflector [37, 38]. Inside a VMI spectrometer, the strongly deflected molecules were aligned using a shaped 250 ps long laser pulse with a peak intensity of $\sim 1.25 \cdot 10^{12} \text{ W/cm}^2$. These pulses

were produced by a commercial laser system (Coherent Legend Elite Duo) with a 1 kHz repetition rate and a spectrum similar to a rounded saw tooth. The pulse was strongly negatively chirped to a duration of ~ 600 ps using a grating based compressor [35] before further shaping. The alignment laser pulses were elliptically polarized with a 3 : 1 intensity ratio between major and minor axes.

The strongly chirped 9 mJ pulses were sent through a zero dispersion $4f$ pulse shaper [39] with a spatial light modulator (SLM, Jenoptik S640d) situated at the Fourier plane in order to generate a truncated pulse with a fast fall-off time. The most relevant part of the shaped temporal intensity profile, around the cutoff, is shown in Figure 2 a. The pulse consisted of a slow rise beginning at -250 ps (not shown), followed by some amplitude modulation, a short kick, and, finally, a fast truncation. The SLM was specifically used for spectral phase modulation of the long-wavelength side of the laser spectrum, i. e., components longer than 815 nm. In addition, wavelengths longer than ~ 816 nm were blocked by a razor blade, situated in front of the SLM. This was necessary due to Nyquist-sampling limits encountered. We note that the combination of phase shaping and spectral truncation with the razor blade improved the temporal fall-off time by a factor of 2.5 down to 3.3 ps, i. e., to within the noise level of the measurement, which was below 1 % of the signal peak, compared to simply cutting the spectrum [32].

The post-pulse observed at ~ 13 ps is unwanted and probably originates from imperfect phase compensation from the SLM or space-time coupling in the pulse shaping setup. However, the post pulse is irrelevant to the degree of alignment within the first 10 ps after the temporal truncation, which corresponds to the important temporal region investigated in this experiment.

A second, time-delayed, laser pulse was used to multiply ionize indole, resulting in Coulomb explosion. These pulses were circularly polarized in order to avoid any secondary dynamics induced by electron rescattering [40] and any additional alignment induced by the probe laser field itself.

Velocity-mapped fragments were detected on a microchannel plate (MCP) detector equipped with a phosphor screen. The voltage on the MCP was switched between 2050 V (MCP “on”) and 1150 V (MCP “off”) using a fast switch (Behlke HTS 31-03-GSM) with 100 ns rise- and fall-times to select the different ion fragments based on their time-of-flight (TOF). A camera (Optonis CL600) recorded single-shot images of the phosphor screen at 200 Hz. Images without pulses from the molecular beam were subtracted from those with the molecular beam to account for any signal from background molecules in the interaction region. After selection of a suitable two-dimensional (2D) radial range, the degree of alignment $\langle \cos^2 \theta_{2D} \rangle$ was computed.

The in-plane principal axes of inertia (a, b) and polarizability (z_I, x_I) are shown in the ball-and-stick represen-

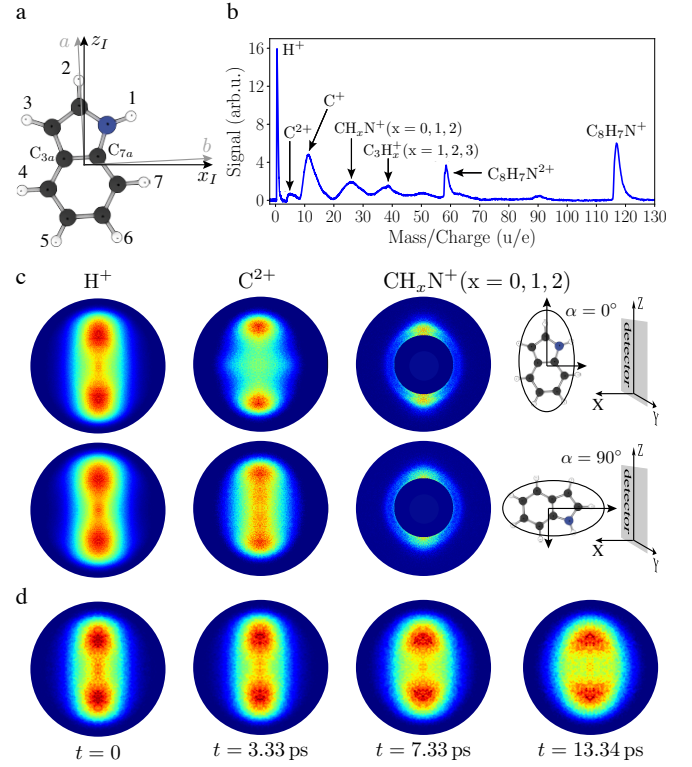


FIG. 1. (a) The structure of indole molecule with its principal axes of inertia and polarizability, labeled by a, b, c and x_I, y_I, z_I ($\alpha_{y_I} < \alpha_{x_I} < \alpha_{z_I}$), respectively. (b) TOF mass spectrum of indole. (c) 2D momentum distributions for H^+ , C^{2+} and CH_xN^+ ($x=0,1,2$) fragments at peak alignment at $t = 3.3$ ps, with the major axis of the alignment laser polarization parallel (first row, $\alpha = 0^\circ$) or perpendicular (second row, $\alpha = 90^\circ$) to the detector plane. (d) Time-snapshots of 2D momentum distributions of H^+ fragments for the case of parallel laser polarization.

tation of indole in Figure 1 a. Both axis frames lie in the plane of the molecule with an angle of 2.75° between them, whereas the c and y_I axes are perpendicular to that plane. Upon Coulomb explosion, several fragmentation channels were detected. The resulting time-of-flight mass spectrum is depicted in Figure 1 b.

Despite the low symmetry of indole, several fragments showed anisotropic momentum distributions. The ion-momentum distributions of H^+ , C^{2+} and CH_xN^+ ($x=0,1,2$) for a delay time of $t = 3.3$ ps, corresponding to the highest observed degree of alignment, are shown in Figure 1 c for two orientations of the alignment laser, i. e., with the main polarization axis being parallel, $\alpha = 0^\circ$, or perpendicular, $\alpha = 90^\circ$, to the plane of the detector. $t = 0$ corresponds to the peak intensity of the alignment laser field. Furthermore, ion-momentum distributions of H^+ for time delays of $t = 0, 3.3, 7.3$, and 13.3 ps are shown in Figure 1 d. The strongest field-free alignment was observed near $t = 3.3$ ps. At later delay times, the dephasing of the rotational wavepacket

leads to a decrease of the molecular alignment, as seen in the momentum distributions recorded at time delays of $t = 7.3$ ps and $t = 13.3$ ps. Momentum distributions of other fragments displaying alignment are shown in the Supplementary Information.

Indole does not contain unique markers, like halogen atoms, which would allow us to easily experimentally access the degree of alignment. Therefore, all ions with a given mass to charge ratio, produced through multiple ionization with subsequent Coulomb explosion, potentially contributed to the measured 2D momentum distributions. There are seven sites in the indole molecule from which the H^+ fragments originate and eight sites for the C^{2+} fragments, see Figure 1 a. Each molecular site will result in different momentum and recoil axis of the ionic fragment, and the total measured distribution is the sum of all of them.

The delay-dependent measured 2D degree of alignment is shown for a variety of fragments in Figure 2. Assuming axial recoil, H^+ fragments would have measurable momentum components only within the ab plane of indole [41]. Hence, the H^+ fragments are *a priori* a good measure of the planar alignment of indole in the laboratory frame. The slow rise of the alignment pulse confined the plane of the indole molecules in a quasi-adiabatic fashion [24, 35] to a measured maximum degree of alignment of $\langle \cos^2 \theta_{2D} \rangle_{H^+}^{\text{exp}} = 0.72$. Following the kick at the end of the alignment pulse, the degree of alignment increased slightly to $\langle \cos^2 \theta_{2D} \rangle_{H^+}^{\text{exp}} = 0.73$ before monotonically decreasing over ~ 10 ps to $\langle \cos^2 \theta_{2D} \rangle_{H^+}^{\text{exp}} = 0.62$. The permanent alignment of $\langle \cos^2 \theta_{2D} \rangle_{H^+}^{\text{exp}} = 0.62$ was slightly higher than the value $\langle \cos^2 \theta_{2D} \rangle_{H^+}^{\text{exp}} = 0.6$ observed without alignment laser; the latter is due to the geometric alignment from an isotropic distribution. At a delay of 3.3 ps the intensity of the alignment pulse decreased to 1 % of its maximum, and the “field-free” region began. At this delay the degree of alignment was $\langle \cos^2 \theta_{2D} \rangle_{H^+}^{\text{exp}} = 0.73$, which was even larger than the alignment measured just before the kick, confirming that the planar alignment in the field-free region was even better than for an adiabatic alignment pulse [42, 43]. All other fragments showed similar distributions to the H^+ fragment, with the measured maximum degree of alignment being largest for the C^{2+} fragment. The differences in the measured alignment between the H^+ , C^+ , C^{2+} and CH_xN^+ ($x=0,1,2$) fragments can be attributed to non-axial recoil or to the geometry of Coulomb explosion fragmentation, i. e., the velocity vectors of the fragments in the molecular frame.

To determine the 3D alignment of indole, an additional observable is required that characterizes the in-plane alignment, i. e., the alignment of the most polarizable axis of indole z_I with respect to the main polarization axis of the alignment field. This information can be accessed by measuring the angular distribution of the ionic fragments within the indole plane. By rotating the polarization el-

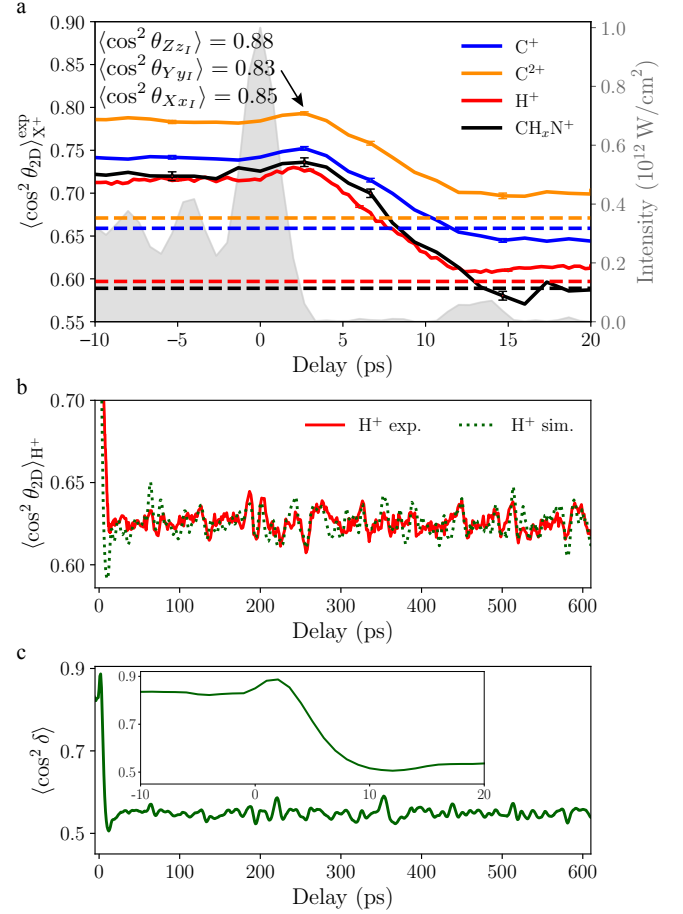


FIG. 2. (a) Temporal evolution of the alignment of indole. The solid lines show the measured 2D degree of alignment $\langle \cos^2 \theta_{2D} \rangle_{X^+}^{\text{exp}}$ for different fragments X^+ and the dashed lines indicate values of the 2D degree of alignment obtained without alignment laser. Statistical error bars, representing the standard error, are shown for selected delays. The grey area shows the intensity profile of the alignment laser pulse. (b) The alignment revival structure of H^+ fragments for longer times is shown in red. The dotted green line shows the fitted simulation for the H^+ fragment. (c) Simulated 3D degree of alignment, characterized through the single-scalar metric $\langle \cos^2 \delta \rangle$, see text/SI for details. Note the peak after truncation reaching $\langle \cos^2 \delta \rangle = 0.89$ at $t = 3.3$ ps.

lipse of the alignment laser around the laser propagation axis at a fixed delay time of 3.3 ps, the laboratory axes to which the a and b axes of indole align, were commensurately rotated. In the laboratory frame, the transverse momenta of ionic fragments recoiling within the plane of indole will depend on the ellipse-rotation angle α , between $\alpha = 0$ for parallel and $\alpha = 90^\circ$ for perpendicular orientation, see Figure 1 c. By counting only those fragments impinging at the center of the detector, within a small radius of 20 pixel, the distribution of fragments within the plane can be determined [44]. Note that the size of the

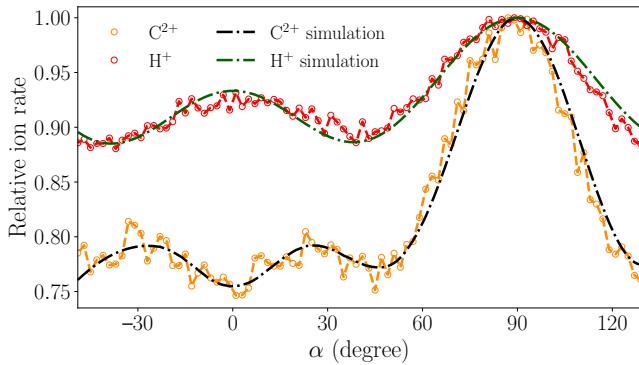


FIG. 3. Measured masked-VMI ion count rates of H^+ and C^{2+} fragments as the major axis of the alignment laser’s polarization ellipse is rotated; see text for details. Circles (red and orange) indicate measured values, the dashed lines (green and black) are simulations based on fitted atomic-ion contributions, see text for details.

VMI images, as shown in Figure 1 c and Figure 1 d, was 480×480 pixels. A full tomographic 3D distribution for $\alpha = 0-180^\circ$ ($\Delta\alpha = 2^\circ$) was obtained from the measurements of H^+ momentum distributions, see Supplementary Information. As no fragments were observed at low 3D momenta, these signals at the center of the VMI can be attributed to in-plane fragments recoiling along the detector normal.

Angular scans of this “masked VMI” are shown in Figure 3 for H^+ and C^{2+} . For both fragments, we observed a clear angle-dependent structure on top of a significant isotropic background. C^{2+} ions show two smaller peaks at $\alpha \approx \pm 30^\circ$ and a much stronger peak at $\alpha \approx 90^\circ$. The H^+ signal shows a peak at $\alpha \approx 90^\circ$, similar to C^{2+} , and a smaller peak at $\alpha \approx 0^\circ$. Note that at 90° the alignment laser’s major polarization axis is pointing along the detector normal. A direct extraction of the in-plane degree of alignment from the experimentally obtained in-plane angular distribution was not possible due to a large isotropic background. Furthermore, the degree of molecular alignment retrieved from the angular momentum distributions of H^+ and C^{2+} can be misrepresented mainly due to two reasons – the many-body Coulomb break-up of the multiply charged indole cation, with ionic fragments violating the axial-recoil approximation, as well as the indistinguishability of fragments emitted at different molecular sites.

In order to extract the actual 3D degree of alignment, we performed comprehensive variational simulations of the rotational dynamics of indole in the presence of the alignment field. We employed the general variational approach RichMol [45, 46] to compute time-dependent rotational probability density distributions for different delay times. In order to incorporate the experimental conditions and to achieve better agreement, we took into account the non-thermal distribution of rotational states

in the deflected part of the molecular beam and laser focal-volume averaging.

The total probability density distributions of C^{2+} and H^+ were modeled as the weighted sums of contributions from the individual atoms. Based on chemical similarity, see Figure 1 a, we used equal weights for pairs of atoms H_1 & H_3 , H_4 & H_7 , H_5 & H_6 , C_{3a} & C_{7a} , C_4 & C_7 , and C_5 & C_6 . As the recoil axes we choose vectors connecting carbon atoms to the center of mass of the molecule for C^{2+} and vectors along molecular C–H and N–H bonds for H^+ . To reproduce the experimental data the simple axial recoil approximation yielded excellent agreement for C^{2+} , whereas for H^+ we had to account for non-axial recoil by convoluting the calculated probability density distributions of hydrogen atoms with a Gaussian function of a solid angle representing angular displacement from the recoil vector. The weights and the FWHM parameter of this Gaussian function were determined in a least-squares fitting procedure to the measured alignment revival trace and the angle-dependent masked VMI data. The obtained parameters are specified in the Supplementary Information. The results of the fit show very good agreement with the experimental alignment revivals in Figure 2 b and excellent agreement with the integrated in-plane angle-dependent projections through the 3D momentum distribution in Figure 3.

This excellent agreement confirms the correct representation of the experiment by our quantum simulations. The obtained planar alignment in terms of squared direction cosines [47] at $t = 3.3$ ps is $\langle \cos^2 \theta_{Y_{yI}} \rangle = 0.83$ and $\langle \cos^2 \theta_{X_{xI}} \rangle = 0.85$. These values are higher than the measured values, which is due to non-axial recoil of the H^+ fragments and different recoil axes contributing to the measured ion-momentum distributions. The computed in-plane degree of alignment at $t = 3.3$ ps is $\langle \cos^2 \theta_{Z_{zI}} \rangle = 0.88$, which we also assign as the experimental value due to the excellent match of the angular distributions in Figure 3. Simulated time-dependent alignment revivals can be found in the Supplementary Information. A single scalar metric describing the overall degree of 3D alignment $\cos^2 \delta = \frac{1}{4}(1 + \cos^2 \theta_{Z_{zI}} + \cos^2 \theta_{Y_{yI}} + \cos^2 \theta_{X_{xI}})$, is shown in Figure 2 c. A maximum degree of field-free alignment of $\langle \cos^2 \delta \rangle = 0.89$ was obtained, which is comparable to or even larger than one can achieve for complex asymmetric top molecules using adiabatic alignment techniques [34, 48] and clearly sufficient for molecular-frame coherent diffractive imaging [18, 19].

In summary, we demonstrated strong laser-field-free 3D alignment of the prototypical complex non-rotation-symmetric molecule indole induced by shaped truncated quasi-adiabatic laser pulses. Both, the amplitude and the phase of a strongly-chirped broad-band alignment laser pulse were tailored using an SLM, which allowed us to produce very short truncation times, unachievable with amplitude truncation alone. The combination of quasi-adiabatic alignment with a kick pulse directly before the

sudden truncation produced a higher degree of alignment under field-free conditions than in the field. The already achieved strong degree of alignment is limited by the initially populated states in the molecular beam [49] and could be further improved through even colder molecular beams [37, 38].

We have developed and tested a new approach to characterize molecular alignment in 3D by performing separate measurements of planar alignment and in-plane tomography. Planar alignment was measured as the time-dependent alignment trace of the H^+ fragments. In-plane alignment was extracted from the angular dependence of H^+ and C^{2+} fragment distributions at the center of the detector, obtained by rotating the laser polarization ellipse and thus the molecule in the plane perpendicular to the detector. Robust variational simulations of the alignment dynamics of indole, considering weighted contributions of fragments emitted non-axially at different molecular sites, reproduced the experiment with high accuracy.

This demonstration of strong field-free alignment for an asymmetric top rotor without rotational symmetries and without any good ionic fragments for the characterization of the alignment paves the way for strong field-free alignment of any arbitrary molecule. This opens up new prospects for probing native (bio)molecules in the molecular frame [19, 20, 50] without chemically attaching marker atoms that influence the function and properties of the molecule.

We thank Stefanie Kerbstadt for helpful discussions. This work has been supported by the Deutsche Forschungsgemeinschaft (DFG) through the priority program “Quantum Dynamics in Tailored Intense Fields” (QUTIF, SPP1840, KU 1527/3, AR 4577/4, YA 610/1) and by the Clusters of Excellence “Center for Ultrafast Imaging” (CUI, EXC 1074, ID 194651731) and “Advanced Imaging of Matter” (AIM, EXC 2056, ID 390715994), and by the European Research Council under the European Union’s Seventh Framework Programme (FP7/2007-2013) through the Consolidator Grant COMOTION (ERC-K pper-614507). J.O. gratefully acknowledges a fellowship of the Alexander von Humboldt Foundation.

Appendix

Fragments of indole showing alignment

In Figure 1, ion-momentum distributions for the H^+ , C^{2+} and $CH_xN^+(x=0,1,2)$ fragments were shown at a delay time of $t = 3.3$ ps, corresponding to the time at which the highest degree of field-free alignment was observed. Further ion-momentum distributions for the same conditions are shown in Figure 4, i. e., for the fragments C^+ , C_2^+ , $C_3H_x^+$, and $C_4H_x^+$, where x depicts fragments with different number of hydrogens whose masses could not be resolved by the high-voltage gating of the detector.

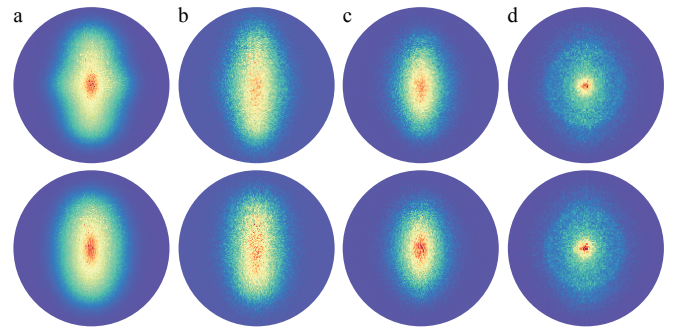


FIG. 4. VMI images of the fragments (a) C^+ , (b) C_2^+ , (c) $C_3H_x^+$, and (d) $C_4H_x^+$. The top row shows images obtained for the major alignment-laser-polarization axis vertical and parallel to the detector surface whereas the bottom row shows corresponding images with the minor alignment-laser-polarization axis vertical and parallel to the detector surface; cf. Figure 1.

Images in the top row show the ion-momentum distributions with the major polarization axis of the alignment laser being parallel and the minor polarization axis being perpendicular to the detector plane ($\alpha = 0^\circ$ in main paper), whereas in the bottom row the major polarization axis is perpendicular and the minor polarization axis is parallel to the detector plane ($\alpha = 90^\circ$ in main paper).

Tomographic reconstruction of H^+ 3D momentum distribution

In Figure 5 isosurfaces of the 3D momentum distribution of H^+ obtained from a tomographic reconstruction of the individual 2D projections measured at a delay time of 3.3 ps are shown. The individual 2D projections were utilized to extract the in-plane distributions in Figure 3. In Figure 5 a the plane spanned by the a and b axes, in Figure 5 b the plane spanned by the a and c axes, and in Figure 5 c the plane spanned by the b and c axes are shown.

Due to the presence of the 2 kV/cm dc field in the interaction point of the VMI spectrometer, minor orientation effects were observed. For the $CH_xN^+(x=0,1,2)$ fragment, a degree of orientation $\langle \cos\theta_{2D} \rangle$ ranging from -0.05 to 0.05 was measured when the laser polarization was rotated by 90° . The 2D ion-momentum distributions of H^+ were thus symmetrized prior to the 3D reconstruction, such that the 3D momentum distributions in Figure 5 represent the average over the four degenerate orientations of indole, which are related via rotations of 180° about the a and b axes.

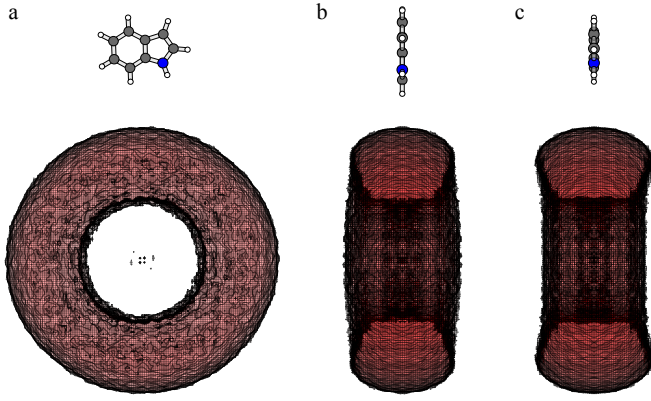


FIG. 5. Reconstructed isosurfaces from H^+ ion-tomography showing three different orientations of the molecule with **a** a-b axes in plane **b** c-a axes in plane **c** c-b axes in plane. The orientation of indole is indicated by the ball-and-stick model of the indole molecule.

Computations

The field-free rotational motion of indole was modelled using the rigid-rotor Hamiltonian with rotational constants $A = 3877.9$ MHz, $B = 1636.1$ MHz, and $C = 1150.9$ MHz [51, 52]. The electric polarizability tensor for the equilibrium molecular geometry was computed *ab initio* at the CCSD/aug-cc-pVTZ [53, 54] level of theory in the frozen core approximation. Electronic structure calculations employed the quantum chemistry package Dalton [55].

Time-dependent quantum dynamics simulations used the general purpose code for quantum mechanical modelling of molecule-field interactions RichMol [45]. In the simulations, the time-dependent wavefunction was built from a superposition of field-free eigenstates and the time-dependent coefficients were obtained by numerically solving the time-dependent Schrödinger equation. The latter was solved using the iterative approximation based on Krylov subspace methods, as implemented in the Expokit computational library [56]. The elliptically polarized alignment laser field was modelled by the function

$$E(t) = E_0(t) \left\{ \mathbf{e}_x \cos(\omega t)/\sqrt{3}, \mathbf{e}_z \sin(\omega t) \right\}, \quad (1)$$

with the electric field amplitude $E_0(t)$ computed from the measured experimental peak intensity. The carrier frequency was fixed to $\omega = c/(2\pi \cdot 800 \text{ nm})$. The time-dependent wavefunction was expressed in the basis of field-free rotational eigenstates of indole with all rotational states with $J \leq 30$ included. The time step used for wavefunction propagation was fixed to 10 fs. Convergence with respect to the size of the rotational basis set and the time step were carefully verified. Since alignment depends nonlinearly on the laser intensity, which is not constant within the focal volume of the laser, integration of all simulated observables over the interaction volume

is required. This has been approximated by repeating the calculations for five individual laser amplitudes, obtained by scaling the originally measured peak intensity $I(t)$ with factors 0.2, 0.4, 0.6, 0.8, and 1.0. The focal volume averaging was carried out using the measured Gaussian beam profiles with widths (FWHM) of $\sigma_{\text{align}} = 56.4 \text{ } \mu\text{m}$ and $\sigma_{\text{probe}} = 28.2 \text{ } \mu\text{m}$. Furthermore, an incoherent average over the initial rotational state distribution, determined from measured experimental deflection profiles, was carried out.

In order to characterize the degree of alignment in the experiment, we computed the rotational probability-density distributions for all hydrogen and carbon atoms in the molecule. The evaluation of the rotational-density functions required the calculation of the Wigner rotation matrices, which was carried out using a Fourier-series based algorithm [57]. For different time delays, two-dimensional projections of the rotational probability density onto the YZ laboratory plane were computed for each atom individually, assuming axial recoil of the hydrogen ions along the C-H and N-H bond vectors, whereas for C^{2+} the vectors connecting the center of mass with each carbon atom were chosen as recoil axes. The 2D projections yielded simulated momentum distributions for all hydrogen atoms, from which the $\langle \cos^2 \theta_{2D} \rangle$ was extracted just the same as from the measured momentum distributions. Furthermore, by rotating the simulated rotational probability-density around the laboratory Y -axis in steps of 1° and carrying out the 2D projection for each rotation angle, the tomography measurements were mimicked. The signal within a radius of 20 pixels was integrated for each angle and for every hydrogen and carbon atom, where both, the experimental and simulated VMI images had a total image size of 480×480 pixels.

Finally, for hydrogens, the weighted simulated alignment traces and the angle-dependent integrated probability density from the center of the detector were simultaneously fitted to the experiment employing least-squares fitting. The resulting time-dependent alignment-revival fit and the angle-dependent integrated probability-density fit are shown in Figure 2 b and Figure 3, respectively. For carbon ions only the integrated probability density was fitted to the experimental data, shown in Figure 3; the corresponding experimental time-dependent alignment trace was too noisy.

The fitting procedures yielded weights representing the contributions of all individual hydrogen and carbon atoms to the measured ion-momentum distributions. Due to the structure of indole, hydrogen atoms that have almost similar angles with respect to the z_I axis of indole, e.g., H_4 & H_7 , see Figure 1 a, result in revivals and angle-dependent probability distributions that are indistinguishable from each other in the experiment. The total probabilities for these equivalent hydrogens were thus summed and calculated to be $P(H_1+H_3) \approx 0.07$, $P(H_2) \approx 0.21$, $P(H_4+H_7) \approx 0.42$, $P(H_5+H_6) \approx 0.30$

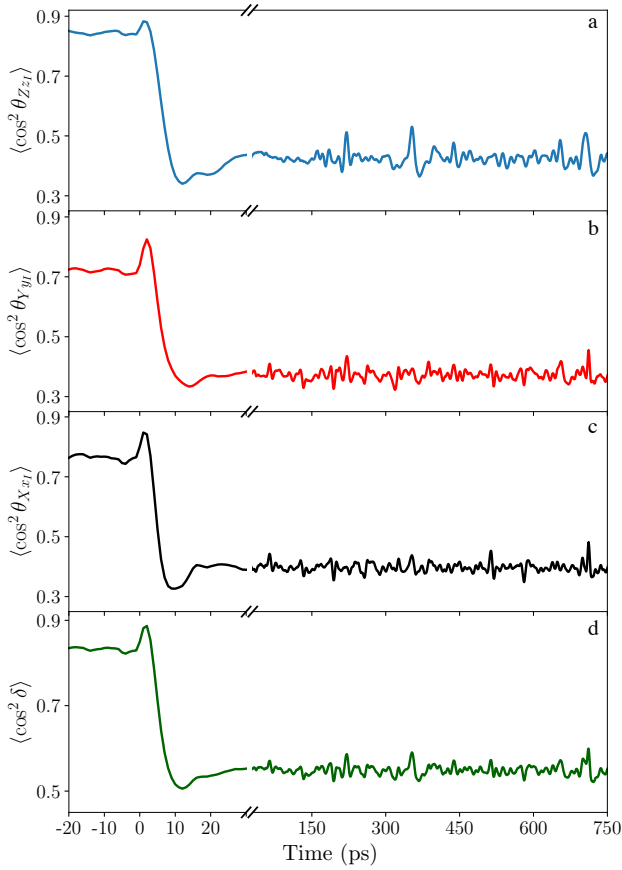


FIG. 6. Simulated degree of 3D alignment characterized through the expectation values (a) $\langle \cos^2 \theta_{Zz_I} \rangle$, (b) $\langle \cos^2 \theta_{Yy_I} \rangle$, (c) $\langle \cos^2 \theta_{Xx_I} \rangle$ and (d) $\langle \cos^2 \delta \rangle$ with the cartesian principal axes of the polarizability tensor frame z_I, y_I, x_I , the cartesian axes of the laboratory-fixed frame X, Y, Z and $\cos^2 \delta = \frac{1}{4}(1 + \cos^2 \theta_{Zz_I} + \cos^2 \theta_{Yy_I} + \cos^2 \theta_{Xx_I})$, a single scalar metric to characterize the 3D alignment [47].

with the squared difference between the experimental and the simulated data $\chi^2_{\min} \approx 0.06$.

For carbon the same procedure yielded $P(C_2) \approx 0.07$, $P(C_3) \approx 0.34$, $P(C_{3a}+C_{7a}) \approx 0.41$, $P(C_4+C_7) \approx 0.06$ and $P(C_5+C_6) \approx 0.12$ with $\chi^2_{\min} \approx 0.017$.

The expectation values of the alignment cosines were computed for the three main polarizability axes in the principle-axis polarizability frame with respect to the laboratory-fixed frame by employing Monte-Carlo integration, converged to better than 10^{-3} using $\sim 10^5$ sampling points. The simulated degree of alignment for the main polarizability axes of the molecule $\alpha_{z_I} > \alpha_{x_I} > \alpha_{y_I}$ with respect to the laboratory axes XYZ is shown in Figure 6. The highest achieved 3D degree of alignment was thus characterized to be $\langle \cos^2 \theta_{Zz_I} \rangle = 0.88$, $\langle \cos^2 \theta_{Yy_I} \rangle = 0.83$, $\langle \cos^2 \theta_{Xx_I} \rangle = 0.85$ and $\langle \cos^2 \delta \rangle = 0.89$, where $\cos^2 \delta = \frac{1}{4}(1 + \cos^2 \theta_{Zz_I} + \cos^2 \theta_{Yy_I} + \cos^2 \theta_{Xx_I})$ [47].

Calculations of the theoretically expected alignment

pulse shape, taking into account SLM pixellation, SLM pixel gaps, the laser beam diameter, and the spectral spread at the Fourier plane, resulted in an expected laser intensity at times between $t = 4$ ps and $t = 10$ ps to be a factor of 70 lower than at the peak of the alignment pulse at $t = 0$ ps.

Finally, we note that further rigid rotor calculations for indole (not shown) indicate that a truncation time of ≤ 2 ps is required to obtain essentially identical dynamics to having an instantaneous truncation. Therefore, phase shaping using the SLM based shaper was highly advantageous, or simply necessary, instead of the more simple frequency filter used in [32], which would result in a 8 ps fall-off in the best case.

* Email: jochen.kuepper@cfel.de; website: <https://www.controlled-molecule-imaging.org>

- [1] Bretislav Friedrich and Dudley Herschbach. Alignment and trapping of molecules in intense laser fields. 74(23): 4623–4626, June 1995. doi:10.1103/PhysRevLett.74.4623.
- [2] Henrik Stapelfeldt and Tamar Seideman. Colloquium: Aligning molecules with strong laser pulses. 75(2):543–557, 2003. doi:10.1103/RevModPhys.75.543. URL <http://link.aps.org/abstract/RMP/v75/p543>.
- [3] S J Weber, M Oppermann, and J P Marangos. Role of rotational wave packets in strong field experiments. 111(26):263601, December 2013. doi:10.1103/PhysRevLett.111.263601. URL <http://link.aps.org/doi/10.1103/PhysRevLett.111.263601>.
- [4] R Torres, N Kajumba, Jonathan G Underwood, J S Robinson, S Baker, J W G Tisch, R de Nalda, W A Bryan, R Velotta, C Altucci, I C E Turcu, and J P Marangos. Probing orbital structure of polyatomic molecules by high-order harmonic generation. 98(20):203007, May 2007. doi:10.1103/PhysRevLett.98.203007. URL <http://link.aps.org/doi/10.1103/PhysRevLett.98.203007>.
- [5] M Meckel, A Staudte, S Patchkovskii, D M Villeneuve, P B Corkum, R Dörner, and M Spanner. Signatures of the continuum electron phase in molecular strong-field photoelectron holography. 10(8):594–600, July 2014. doi:10.1038/nphys3010. URL <https://www.nature.com/articles/nphys3010>.
- [6] Domagoj Pavičić, Kevin F. Lee, D. M. Rayner, P. B. Corkum, and D. M. Villeneuve. Direct measurement of the angular dependence of ionization for N₂, O₂, and CO₂ in intense laser fields. 98:243001, Jun 2007. doi:10.1103/PhysRevLett.98.243001. URL <https://link.aps.org/doi/10.1103/PhysRevLett.98.243001>.
- [7] Andrea Trabattini, Joss Wiese, Umberto De Giovannini, Jean-François Olivieri, Terry Mullins, Jolijn Onvlee, Sang-Kil Son, Biagio Frusteri, Angel Rubio, Sebastian Trippel, and Jochen Küpper. Setting the photoelectron clock through molecular alignment. 11:2546, May 2020. doi:10.1038/s41467-020-16270-0. URL <https://doi.org/10.1038/s41467-020-16270-0>.
- [8] Jochen Küpper, Stephan Stern, Lotte Holmegaard, Frank Filsinger, Arnaud Rouzée, Artem Rudenko, Per Johnsson, Andrew V. Martin, Marcus Adolph, Andrew Aquila,

- Saša Bajt, Anton Barty, Christoph Bostedt, John Bozek, Carl Caleman, Ryan Coffee, Nicola Coppola, Tjark Demas, Sascha Epp, Benjamin Erk, Lutz Foucar, Tais Gorkhover, Lars Gumprecht, Andreas Hartmann, Robert Hartmann, Günter Hauser, Peter Holl, Andre Hömke, Nils Kimmel, Faton Krasniqi, Kai-Uwe Kühnel, Jochen Maurer, Marc Messerschmidt, Robert Moshhammer, Christian Reich, Benedikt Rudek, Robin Santra, Ilme Schlichting, Carlo Schmidt, Sebastian Schorb, Joachim Schulz, Heike Soltau, John C. H. Spence, Dmitri Starodub, Lothar Strüder, Jan Thøgersen, Marc J. J. Vrakking, Georg Weidenspointner, Thomas A. White, Cornelia Wunderer, Gerard Meijer, Joachim Ullrich, Henrik Stapelfeldt, Daniel Rolles, and Henry N. Chapman. X-ray diffraction from isolated and strongly aligned gas-phase molecules with a free-electron laser. 112:083002, 2014. doi:10.1103/PhysRevLett.112.083002. URL <https://dx.doi.org/10.1103/PhysRevLett.112.083002>.
- [9] Thomas Kierspel, Andrew Morgan, Joss Wiese, Terry Mullins, Andy Aquila, Anton Barty, Richard Bean, Rebecca Boll, Sébastien Boutet, Philip Bucksbaum, Henry N. Chapman, Lauge Christensen, Alan Fry, Mark Hunter, Jason E Koglin, Mengning Liang, Valerio Mariani, Adi Natan, Joseph Robinson, Daniel Rolles, Artem Rudenko, Kirsten Schnorr, Henrik Stapelfeldt, Stephan Stern, Jan Thøgersen, Chun Hong Yoon, Fenglin Wang, and Jochen Küpper. X-ray diffractive imaging of controlled gas-phase molecules: Toward imaging of dynamics in the molecular frame. 152(8):084307, February 2020. doi:10.1063/1.5133963. URL <https://doi.org/10.1063/1.5133963>.
- [10] M. Meckel, D. Comtois, D. Zeidler, A. Staudte, D. Pavičić, H. C. Bandulet, H. Pépin, J. C. Kieffer, R. Dörner, D. M. Villeneuve, and P. B. Corkum. Laser-induced electron tunneling and diffraction. *Science*, 320(5882):1478–1482, 2008. ISSN 0036-8075. doi:10.1126/science.1157980. URL <http://science.sciencemag.org/content/320/5882/1478>.
- [11] S G Walt, B N Ram, M Atala, N I Shvetsov-Shilovski, A von Conta, D Baykusheva, M Lein, and H J Wörner. Dynamics of valence-shell electrons and nuclei probed by strong-field holography and rescattering. 8:15651, 2017. doi:10.1038/ncomms15651. URL <https://www.nature.com/articles/ncomms15651>.
- [12] Michael G. Pullen, Benjamin Wolter, Anh-Thu Le, Matthias Baudisch, Michael Hemmer, Arne Senftleben, Claus Dieter Schroter, Joachim Ullrich, Robert Moshhammer, C. D. Lin, and Jens Biegert. Imaging an aligned polyatomic molecule with laser-induced electron diffraction. *Nat. Commun.*, 6:7262, 2015. doi:10.1038/ncomms8262. URL <http://www.nature.com/ncomms/2015/150624/ncomms8262/full/ncomms8262.html>.
- [13] Christopher J. Hensley, Jie Yang, and Martin Centurion. Imaging of isolated molecules with ultrafast electron pulses. 109:133202, 2012. doi:10.1103/PhysRevLett.109.133202. URL <https://dx.doi.org/10.1103/PhysRevLett.109.133202>.
- [14] Jie Yang, Markus Guehr, Theodore Vecchione, Matthew S. Robinson, Renkai Li, Nick Hartmann, Xiaozhe Shen, Ryan Coffee, Jeff Corbett, Alan Fry, Kelly Gaffney, Tais Gorkhover, Carsten Hast, Keith Jobe, Igor Makasyuk, Alexander Reid, Joseph Robinson, Sharon Vetter, Fenglin Wang, Stephen Weathersby, Charles Yoneda, Martin Centurion, and Xijie Wang. Diffractive imaging of a rotational wavepacket in nitrogen molecules with femtosecond megaelectronvolt electron pulses. 7:11232, April 2016. doi:10.1038/ncomms11232. URL <http://dx.doi.org/10.1038/ncomms11232>.
- [15] J. Itatani, J. Levesque, D. Zeidler, H. Niikura, H. Pépin, J. C. Kieffer, P. B. Corkum, and D. M. Villeneuve. Tomographic imaging of molecular orbitals. 432:867–871, 2004. doi:10.1038/nature03183. URL <https://dx.doi.org/10.1038/nature03183>.
- [16] Lotte Holmegaard, Jonas L. Hansen, Line Kalhøj, Sofie Louise Kragh, Henrik Stapelfeldt, Frank Filsinger, Jochen Küpper, Gerard Meijer, Darko Dimitrovski, Mahmoud Abu-samha, Christian P. J. Martiny, and Lars Bojer Madsen. Photoelectron angular distributions from strong-field ionization of oriented molecules. *Nat. Phys.*, 6:428, 2010. doi:10.1038/NPHYS1666. URL <https://www.nature.com/articles/nphys1666>.
- [17] C. Vozzi, M. Negro, F. Calegari, G. Sansone, M. Nisoli, S. De Silvestri, and S. Stagira. Generalized molecular orbital tomography. 7:822–826, June 2011. doi:10.1038/nphys2029.
- [18] Frank Filsinger, Gerard Meijer, Henrik Stapelfeldt, Henry Chapman, and Jochen Küpper. State- and conformer-selected beams of aligned and oriented molecules for ultrafast diffraction studies. 13(6):2076–2087, 2011. doi:10.1039/C0CP01585G. URL <https://dx.doi.org/10.1039/C0CP01585G>.
- [19] Anton Barty, Jochen Küpper, and Henry N. Chapman. Molecular imaging using x-ray free-electron lasers. 64(1):415–435, April 2013. doi:10.1146/annurev-physchem-032511-143708. URL <http://dx.doi.org/10.1146/annurev-physchem-032511-143708>.
- [20] John C. H. Spence and R. Bruce Doak. Single molecule diffraction. 92(19):198102, Jan 2004. doi:10.1103/PhysRevLett.92.198102. URL <http://prola.aps.org/abstract/PRL/v92/i19/e198102>.
- [21] Linda V Thesing, Jochen Küpper, and Rosario González-Férez. Time-dependent analysis of the mixed-field orientation of molecules without rotational symmetry. 146(24):244304, June 2017. doi:10.1063/1.4986954. URL <https://doi.org/10.1063/1.4986954>.
- [22] W. Gordy and R. L. Cook. *Microwave Molecular Spectra*. New York, NY, USA, 3 edition, 1984.
- [23] F Rosca-Pruna and Marc J. J Vrakking. Experimental observation of revival structures in picosecond laser-induced alignment of I₂. 87(15):153902, January 2001. doi:10.1103/PhysRevLett.87.153902. URL <http://prola.aps.org/abstract/PRL/v87/i15/e153902>.
- [24] Sebastian Trippel, Terence Mullins, N L M Müller, Jens S Kienitz, Juan J Omiste, Henrik Stapelfeldt, Rosario González-Férez, and Jochen Küpper. Strongly driven quantum pendulum of the carbonyl sulfide molecule. 89:051401(R), 2014. doi:10.1103/PhysRevA.89.051401. URL <https://journals.aps.org/pra/abstract/10.1103/PhysRevA.89.051401>.
- [25] S. Trippel, T. Mullins, N. L. M. Müller, J. S. Kienitz, R. González-Férez, and J. Küpper. Two-state wave packet for strong field-free molecular orientation. 114:103003, 2015. doi:10.1103/PhysRevLett.114.103003. URL <https://dx.doi.org/10.1103/PhysRevLett.114.103003>.
- [26] Evangelos T. Karamatskos, Sebastian Raabe, Terry Mullins, Andrea Trabatttoni, Philipp Stammer, Gildas Goldsztejn, Rasmus R. Johansen, Karol Długołęcki, Henrik Stapelfeldt, Marc. J. J. Vrakking, Sebastian Trippel, Arnaud Rouzée, and Jochen Küpper. Molec-

- ular movie of ultrafast coherent rotational dynamics of OCS. *Nat. Commun.*, 10:3364, 2019. doi: 10.1038/s41467-019-11122-y. URL <https://dx.doi.org/10.1038/s41467-019-11122-y>.
- [27] J. J. Larsen, K. Hald, N. Bjerre, H. Stapelfeldt, and T. Seideman. Three dimensional alignment of molecules using elliptically polarized laser fields. 85:2470–2473, 2000. doi:10.1103/PhysRevLett.85.2470.
- [28] H. Tanji, S. Minemoto, and H. Sakai. Three-dimensional molecular orientation with combined electrostatic and elliptically polarized laser fields. 72:063401, 2005. doi: 10.1103/PhysRevA.72.063401.
- [29] Iftach Nevo, Lotte Holmegaard, Jens H. Nielsen, Jonas L. Hansen, Henrik Stapelfeldt, Frank Filsinger, Gerard Meijer, and Jochen Küpper. Laser-induced 3D alignment and orientation of quantum state-selected molecules. 11: 9912–9918, 2009. doi:10.1039/b910423b.
- [30] Daisuke Takei, Je Hoi Mun, Shinichirou Minemoto, and Hirofumi Sakai. Laser-field-free three-dimensional molecular orientation. 94:013401, 2016. doi: 10.1103/PhysRevA.94.013401. URL <https://journals.aps.org/prapdf/10.1103/PhysRevA.94.013401>.
- [31] Thomas Kierspel, Joss Wiese, Terry Mullins, Joseph Robinson, Andy Aquila, Anton Barty, Richard Bean, Rebecca Boll, Sébastien Boutet, Philip Bucksbaum, Henry N. Chapman, Lauge Christensen, Alan Fry, Mark Hunter, Jason E. Koglin, Mengning Liang, Valerio Mariani, Andrew Morgan, Adi Natan, Vladimir Petrovic, Daniel Rolles, Artem Rudenko, Kirsten Schnorr, Henrik Stapelfeldt, Stephan Stern, Jan Thøgersen, Chun Hong Yoon, Fenglin Wang, Sebastian Trippel, and Jochen Küpper. Strongly aligned molecules at free-electron lasers. 48(20):204002, 2015. doi:10.1088/0953-4075/48/20/204002.
- [32] A.S. Chatterley, Evangelos T. Karamatskos, Constant Schouder, Lars Christiansen, Anders V. Jørgensen, Terry Mullins, Jochen Küpper, and Henrik Stapelfeldt. Switched wave packets with spectrally truncated chirped pulses. 148:221105, 2018. doi:10.1063/1.5028359. URL <https://doi.org/10.1063/1.5028359>.
- [33] Adam S. Chatterley, Constant Schouder, Lars Christiansen, Benjamin Shepperson, Mette Heidemann Rasmussen, and H. Stapelfeldt. Long-lasting field-free alignment of large molecules inside helium nanodroplets. 10 (133):073202, 2019. doi:10.1038/s41467-018-07995-0. URL <https://doi.org/10.1038/s41467-018-07995-0>.
- [34] Jonas L Hansen, Juan J Omiste, Jens Hedegaard Nielsen, Dominik Pentlechner, Jochen Küpper, Rosario González-Férez, and Henrik Stapelfeldt. Mixed-field orientation of molecules without rotational symmetry. 139:234313, 2013. doi:10.1063/1.4848735.
- [35] Sebastian Trippel, Terry Mullins, Nele L. M. Müller, Jens S. Kienitz, Karol Długołęcki, and Jochen Küpper. Strongly aligned and oriented molecular samples at a kHz repetition rate. *Mol. Phys.*, 111:1738, 2013. doi:10.1080/00268976.2013.780334. URL <http://dx.doi.org/10.1080/00268976.2013.780334>.
- [36] U. Even, J. Jortner, D. Noy, N. Lavie, and N. Cossart-Magos. Cooling of large molecules below 1 K and He clusters formation. 112:8068–8071, 2000. doi: 10.1063/1.481405. URL <http://dx.doi.org/10.1063/1.481405>.
- [37] Frank Filsinger, Jochen Küpper, Gerard Meijer, Lotte Holmegaard, Jens H. Nielsen, Iftach Nevo, Jonas L. Hansen, and Henrik Stapelfeldt. Quantum-state selection, alignment, and orientation of large molecules using static electric and laser fields. 131:064309, 2009. doi: 10.1063/1.3194287. URL <http://scitation.aip.org/content/aip/journal/jcp/131/6/10.1063/1.3194287>.
- [38] Yuan-Pin Chang, Daniel A. Horke, Sebastian Trippel, and Jochen Küpper. Spatially-controlled complex molecules and their applications. *Int. Rev. Phys. Chem.*, 34:557–590, 2015. doi:10.1080/0144235X.2015.1077838. URL <https://dx.doi.org/10.1080/0144235X.2015.1077838>.
- [39] A. M. Weiner, D. E. Leaird, J. S. Patel, and J. R. Wullert. Programmable shaping of femtosecond optical pulses by use of 128-element liquid crystal phase modulator. *IEEE Journal of Quantum Electronics*, 28(4):908–920, April 1992. doi:10.1109/3.135209. URL <https://ieeexplore.ieee.org/document/135209/>.
- [40] H. Niikura, F. Légaré, R. Hasbani, A. D. Bandrauk, M. Y. Ivanov, D. M. Villeneuve, and P. B. Corkum. Sub-laser-cycle electron pulses for probing molecular dynamics. 417: 917–922, 2002. doi:10.1038/nature00787. URL <https://www.nature.com/articles/nature00787>.
- [41] E. Kukk, H. Myllynen, K. Nagaya, S. Wada, J. D. Bozek, T. Takanashi, D. You, A. Niozu, K. Kooser, T. Gaumnitz, E. Pelimanni, M. Berholts, S. Granroth, N. Yokono, H. Fukuzawa, C. Miron, and K. Ueda. Coulomb implosion of tetrabromothiophene observed under multiphoton ionization by free-electron-laser soft-x-ray pulses. 99:023411, Feb 2019. doi:10.1103/PhysRevA.99.023411. URL <https://link.aps.org/doi/10.1103/PhysRevA.99.023411>.
- [42] S. Guérin, A. Rouzée, and E. Hertz. Ultimate field-free molecular alignment by combined adiabatic-impulsive field design. 77(4):041404, April 2008. doi: 10.1103/PhysRevA.77.041404. URL <http://link.aps.org/doi/10.1103/PhysRevA.77.041404>.
- [43] Arnaud Rouzée, Edouard Hertz, Bruno Lavorel, and Olivier Faucher. Towards the adaptive optimization of field-free molecular alignment. 41(7):074002, April 2008. doi:10.1088/0953-4075/41/7/074002. URL <http://iopscience.iop.org/article/10.1088/0953-4075/41/7/074002>.
- [44] D. M. Villeneuve, S.A. Aseyev, A. Avery, and P. B. Corkum. Using frequency-domain manipulation of stretched femtosecond laser pulses to create fast rise and fall times on picosecond pulses. 74:S157 – S161, 2002. doi:10.1007/s00340-002-0899-3.
- [45] Alec Owens and Andrey Yachmenev. RichMol: A general variational approach for rovibrational molecular dynamics in external electric fields. 148(12):124102, March 2018. doi:10.1063/1.5023874. URL <https://doi.org/10.1063/1.5023874>.
- [46] Andrey Yachmenev, Linda V. Thesing, and Jochen Küpper. Laser-induced dynamics of molecules with strong nuclear quadrupole coupling. 151(24):244118, 2019. doi: 10.1063/1.5133837. URL <https://doi.org/10.1063/1.5133837>.
- [47] Varun Makhija, Xiaoming Ren, and Vinod Kumarappan. Metric for three-dimensional alignment of molecules. 85:033425, Mar 2012. doi: 10.1103/PhysRevA.85.033425. URL <https://link.aps.org/doi/10.1103/PhysRevA.85.033425>.
- [48] Sebastian Trippel, Joss Wiese, Terry Mullins, and Jochen Küpper. Communication: Strong laser alignment of solvent-solute aggregates in the gas-phase. 148(10): 101103, March 2018. doi:10.1063/1.5023645. URL <http://aip.scitation.org/doi/10.1063/1.5023645>.

- [49] Vinod Kumarappan, Christer Z Bisgaard, Simon S Viftrup, Lotte Holmegaard, and Henrik Stapelfeldt. Role of rotational temperature in adiabatic molecular alignment. 125(19):194309, Jan 2006. doi:10.1063/1.2388273.
- [50] Nicole Teschmit, Daniel A. Horke, and Jochen Küpper. Spatially separating the conformers of a dipeptide. 57(42): 13775–13779, October 2018. doi:10.1002/anie.201807646. URL <https://onlinelibrary.wiley.com/doi/abs/10.1002/anie.201807646>.
- [51] G. Berden, W. L. Meerts, and E. Jalviste. Rotationally resolved ultraviolet spectroscopy of indole, indazole, and benzimidazole: Inertial axis reorientation in the $S_1(^1L_b) \leftarrow S_0$ transitions. 103:9596–9606, 1995. doi: 10.1063/1.469974. URL <https://doi.org/10.1063/1.469974>.
- [52] Cheolhwa Kang, Timothy M. Korter, and David W. Pratt. Experimental measurement of the induced dipole moment of an isolated molecule in its ground and electronically excited states: Indole and indole-H₂O. 122(17):174301, 2005. doi:10.1063/1.1883635. URL <https://doi.org/10.1063/1.1883635>.
- [53] T. H. Dunning. Gaussian basis sets for use in correlated molecular calculations. I. The atoms boron through neon and hydrogen. 90:1007, 1989. doi:10.1063/1.456153. URL <https://dx.doi.org/10.1063/1.456153>.
- [54] Rick A. Kendall, Thom H. Dunning, Jr., and Robert J. Harrison. Electron affinities of the first-row atoms revisited. Systematic basis sets and wave functions. 96(9):6796–6806, 1992. doi:10.1063/1.462569. URL <http://dx.doi.org/10.1063/1.462569>.
- [55] Kęstutis Aidas, Celestino Angeli, Keld L. Bak, Vebjørn Bakken, Radovan Bast, Linus Boman, Ove Christiansen, Renzo Cimiraglia, Sonia Coriani, Pål Dahle, Erik K. Dalskov, Ulf Ekström, Thomas Enevoldsen, Janus J. Eriksen, Patrick Ettenhuber, Berta Fernández, Lara Ferrihi, Heike Fliegl, Luca Frediani, Kasper Hald, Asger Halkier, Christof Hättig, Hanne Heiberg, Trygve Helgaker, Alf Christian Hennum, Hinne Hettema, Eirik Hjertenæs, Stinne Høst, Ida-Marie Høyvik, Maria Francesca Iozzi, Branislav Jansík, Hans Jørgen Aa. Jensen, Dan Jonsen, Poul Jørgensen, Joanna Kauczor, Sheela Kirpekar, Thomas Kjærgaard, Wim Klopper, Stefan Knecht, Rika Kobayashi, Henrik Koch, Jacob Kongsted, Andreas Krapp, Kasper Kristensen, Andrea Ligabue, Ola B Lutnæs, Juan I. Melo, Kurt V. Mikkelsen, Rolf H. Myhre, Christian Neiss, Christian B. Nielsen, Patrick Norman, Jeppe Olsen, Jógvan Magnus H. Olsen, Anders Osted, Martin J. Packer, Filip Pawłowski, Thomas B. Pedersen, Patricio F. Provasi, Simen Reine, Zilvinas Rinkevicius, Torgeir A. Ruden, Kenneth Ruud, Vladimir V. Rybkin, Pawel Salek, Claire C. M. Samson, Alfredo Sánchez de Merás, Trond Saue, Stephan P. A. Sauer, Bernd Schimmelpfennig, Kristian Sneskov, Arnfinn H. Steindal, Kristian O. Sylvester-Hvid, Peter R. Taylor, Andrew M. Teale, Erik I. Tellgren, David P. Tew, Andreas J. Thorvaldsen, Lea Thøgersen, Olav Vahtras, Mark A. Watson, David J. D. Wilson, Marcin Ziolkowski, and Hans Ågren. The Dalton quantum chemistry program system. *WIREs Comput. Mol. Sci.*, 4(3):269–284, 2014. doi:10.1002/wcms.1172.
- [56] Roger B. Sidje. Expokit: a software package for computing matrix exponentials. *ACM Transactions on Mathematical Software*, 24(1):130–156, March 1998. doi: 10.1145/285861.285868.
- [57] Naoki Tajima. Analytical formula for numerical evaluations of the Wigner rotation matrices at high spins. 91: 014320, January 2015. doi:10.1103/PhysRevC.91.014320. URL <http://link.aps.org/doi/10.1103/PhysRevC.91.014320>.